Textile composite structural analysis taking into account the forming process

Abderrahmen Aridhi, Makrem Arfaoui, Tarek Mabrouki, Naïm Naouar, Yvan Denis, Malek Zarroug, Philippe Boisse

Accepted Manuscript

Textile composite structural analysis taking into account the forming process

Abderrahmen Aridhi, Makrem Arfaoui, Tarek Mabrouki, Naim Naouar, Yvan Denis, Malek Zarroug, Philippe Boisse

PII: S1359-8368(18)34265-3

DOI: https://doi.org/10.1016/j.compositesb.2019.02.047

Reference: JCOMB 6633

To appear in: *Composites Part B*

Received Date: 8 December 2018

Revised Date: 26 January 2019

Accepted Date: 12 February 2019

Please cite this article as: Aridhi A, Arfaoui M, Mabrouki T, Naouar N, Denis Y, Zarroug M, Boisse P, Textile composite structural analysis taking into account the forming process, *Composites Part B* (2019), doi: https://doi.org/10.1016/j.compositesb.2019.02.047.

Textile composite structural analysis taking into account the forming process

Abderrahmen Aridhi[a,b], Makrem Arfaoui[b], Tarek Mabrouki[b], Naim Naouar[a], Yvan Denis[a], Malek Zarroug[c], Philippe Boisse[a,*]

[a] *Universit de Lyon, CNRS, INSA-Lyon, LaMCoS, F69621, France*
[b] *Universit de Tunis El Manar, ENIT, Mcanique Applique et Ingnierie, LR11ES19, 1002, Tunis, Tunisie*
[c] *Direction Scientique et Technologies Futures, PSA Peugeot socit anonyme, 78140 Vlizy-Villacoublay, France*

Abstract

The manufacturing processes of composite materials modify the internal structure and therefore the mechanical properties of cured composite parts. In particular, draping of woven prepregs leads to angle changes between warp and weft yarns when the geometry of the part is double curved. We were propose to take the fiber reorientation caused by forming into account the structural analysis of a cured composite. For this purpose, the simulation for the forming of prepregs was based on a rate constitutive equation. Then, a simple orthotropic elastic model of the cured composite was developed to take into account the angle change created by the forming. An experimental validation of this approach was performed in the case of traction on a cured test specimen after a bias extension test. Structural analyses of 3D composite parts obtained by draping also showed that it was necessary to take into account the reorientation of the fibers.

Keywords: Fabrics/textilles; Mechanical properties; Finite element analysis (FEA); Forming; Fiber reorientation

1. Introduction

The automotive industry must currently reconcile two limitations. The first one is the reduction of polluting emissions by decreasing the vehicle weights. For this, the use of composite materials is one of the main solutions. The second challenge requires improving the production rate and the mechanical properties of the composite parts [1–5]. In this context, the use of materials made of continuous fibers in a thermoplastic matrix shaped by thermo-stamping, constitutes a good compromise between mechanical performance, cost and production rate. In particular, woven textile composites can be readily shaped and also draped on complex forms. For double curve geometries, textile composites are efficient thanks to the interlacing of warp and weft yarns. Moreover, the thermoplastic matrix can be recyclable which is an important advantage for the automotive industry.

*Corresponding author
Email address: philippe.boisse@insa-lyon.fr (Philippe Boisse)

Figure 1: Stages of the thermoforming process

In the composite thermoforming process, the thermoplastic prepreg is first heated at a temperature slightly higher than the fusion point of the matrix (Figure 1). It is then conveyed into a mold that is at a temperature lower than that of the prepreg. The mold closes and shapes the composite part. After a consolidation phase, the composite part is cooled in ambient air [6–12]. This manufacturing process only lasts a few tens of seconds. The composite part can then be used and subjected to structural forces.

The forming process changes the state of the prepreg: in particular, the fiber directions are modified. In the case of woven reinforcements, the in-plane shear strain due to the shaping corresponds to changes in the angles between the weft and warp yarns. In addition, certain defects may develop during thermoforming, and wrinkles are one of the major issues [13–18]. Slippage between warp and weft yarns may also occur [19]. These defects can be minimized by optimizing process parameters through simulation.

This article analyzes the influence of the angle change due to thermoforming on the mechanical properties of the final composite part. A simulation of the forming based on a hypoelastic constitutive law made it possible to determine the angle changes between the warp and weft yarns. A simple model was used to take into account angle changes in the mechanical behavior of the final hardened composite. A bias extension test on a hardened composite specimen was performed experimentally, and by comparing experimental and simulated results, the model could be validated. The forming of a hemisphere with a non-symmetric blank holder showed the importance of taking into account the angle changes between the warp and weft yarns in the structural analysis of the cured composite.

2. Simulation of the forming process

There are two main approaches for simulating the draping of woven reinforcements. The first one is based on the so-called kinematic model, where the yarns are considered to be pinned together at the crossover points of the weave [20–22]. This simple approach is widely used because it requires only a short calculation time and it is fairly efficient especially in the case of manually operated prepreg draping.

An alternative approach is based on continuum mechanics associated with Finite Element Analysis [23–26]. According to the multiscale nature of the woven composites, the FE models can be performed at different scales. The micro-scale models analyze the reinforcement by considering that each fiber is in contact with its neighbors [27–31]. The mesoscopic models, developed at the meso-scale, consider the woven fabric as a set of yarns in contact and each yarn as a continuous medium [32–37]. The macroscopic analyses consider the whole reinforcement as a continuous medium. This macroscopic approach is the most commonly

used in composite forming simulations. The reinforcement/prepreg composite is not continuous at lower scales but, in most cases, a continuous material superimposed on average with textile reinforcement can be considered at macroscopic scale. The macroscopic approaches can be implemented in FE codes using standard elements. Different macroscale models have been developed [38–45], of which some are based on hyperelastic formulations where the constitutive model is derived from a potential energy [46–48].

Another group of models relies on hypoelastic formulation (or rate constitutive equations) where a Cauchy objective stress derivative is related to the strain rate by a constitutive tensor. The rate constitutive models are widely used for large strain analysis [49, 50], and the forming simulation presented below is based on this hypoelastic approach. Commercial finite element simulation programs use by default a rate constitutive equation or hypoelastic law, especially in user routines such as UMAT or VUMAT (Abaqus). In this context, it is natural to develop a rate constitutive law specific to textile reinforcements as done in this article. In addition, hypoelastic laws use a classical behaviour matrix that links the stress increment and the deformation increment. The quantities to be identified are Young's moduli and shear moduli whose meaning is clear.

2.1. Constitutive model for woven fabrics: Hypoelastic formulation

The hypoelastic approaches are used in case of geometrical non-linearities and elastic non-linear behaviors. Several rate constitutive models have been developed for woven textile forming simulation. Peng and Cao [51] and Yu et al, [52] developed non orthogonal models. Boisse et al, [53–55] introduced a specific hypoelastic model at the meso-scale where the rotated frame was defined by the rotation of the fiber. This meso approach was used in analyses of the unit woven cell made of fiber bundle where all the fibers were juxtaposed and parallel. Consequently, there was only one fiber direction at the current point of the material. Khan et al. [56] extended this approach to the macroscopic level in order to simulate fabric/prepreg forming processes (i.e with warp and weft yarns). In this model there are two fiber directions in a point, respecting the warp and weft directions.

A hypoelastic constitutive law relates an objective derivative of the Cauchy stress tensor $\underline{\underline{\sigma}}^{\nabla}$ to the strain rate $\underline{\underline{D}}$ by a constitutive tensor $\underline{\underline{\underline{\underline{C}}}}$.

$$\underline{\underline{\sigma}}^{\nabla} = \underline{\underline{\underline{\underline{C}}}} : \underline{\underline{D}} \tag{1}$$

The objective derivative can be considered as a derivative for an observer who is in a fixed position with regard to the material orientation. The objective derivative is used at large strains to avoid stress change caused by rigid body rotations when considering $\dot{\underline{\underline{\sigma}}} = \frac{d\underline{\underline{\sigma}}}{dt}$ [49, 50]. The presented model exploits an objective derivative based on the fiber rotation tensor $\underline{\underline{\Delta}}$ which is the rotation from the initial to the current fiber direction. Then, the objective derivative of the Cauchy stress tensor has the following expression:

$$\underline{\underline{\sigma}}^{\nabla} = \underline{\underline{\Delta}} \left(\frac{d}{dt} \left(\underline{\underline{\Delta}}^T . \underline{\underline{\sigma}} . \underline{\underline{\Delta}} \right) \right) \underline{\underline{\Delta}}^T \tag{2}$$

If the corresponding spin is denoted $\underline{\underline{\Omega}} = \dot{\underline{\underline{\Delta}}} . \underline{\underline{\Delta}}^T$, the objective Cauchy stress derivative can be written:

$$\underline{\underline{\sigma}}^{\nabla} = \dot{\underline{\underline{\sigma}}} + \underline{\underline{\sigma}} \cdot \underline{\underline{\Omega}} - \underline{\underline{\Omega}} \cdot \underline{\underline{\sigma}} \tag{3}$$

Several objective derivatives are classically defined from different rotation tensors. In particular,

- The Jauman objective derivative: based on the rotation tensor $\underline{\underline{R'}}_s$ of the corotational frame (spinless)[57].
- The Green Naghdi objective derivative: based on the polar rotation $\underline{\underline{R}}$ obtained by the polar decomposition of the gradient tensor $\underline{\underline{F}} = \underline{\underline{R}}.\underline{\underline{U}}$, where $\underline{\underline{U}}$ is the right stretch tensor [58].

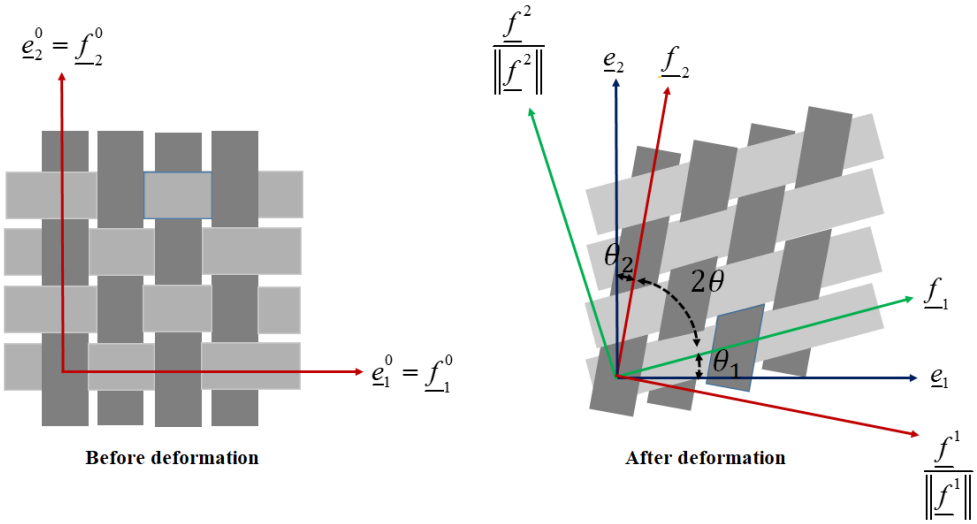

Figure 2: Schematic of a deformed plain weave structure

2.2. Stress update using a hypoelastic law for woven reinforcement

The unit vectors $\underline{f}_1$ and $\underline{f}_2$ coincide with the current directions of warp and weft (Figure 2). Let $\underline{f}_1^0$ and $\underline{f}_2^0$ denote the fiber directions in the initial configuration. They are are orthogonal. In the current configuration, the fiber directions are obtained from the deformation gradient tensor $\underline{\underline{F}}$ and the initial fiber directions

$$\underline{f}_i = \frac{\underline{\underline{F}}.\underline{f}_i^0}{\left\|\underline{\underline{F}}.\underline{f}_i^0\right\|} \quad i = 1, 2 \tag{4}$$

The frame $\left(\underline{f}_1, \underline{f}_2\right)$ is not orthonormal. The contravariant assocciated vectors $\left(\underline{f}^1, \underline{f}^2\right)$ are defined as:

$$\underline{f}_i.\underline{f}^j = \delta_i^j \quad i = 1, 2 \tag{5}$$

It is possible in Abaqus/Explicit to use a user subroutine (VUMAT) to introduce a specific behavior law. This is how the hypoelastic law described in this section is implemented. In this user subroutine, the components of the different tensors are expressed in the Green Naghdi frame (GN). This frame is entrained by the rotation of the polar decomposition $\underline{\underline{F}} = \underline{\underline{R}} \cdot \underline{\underline{U}}$. In the current configuration, the Green Naghdi vectors $\underline{e}_1$ and $\underline{e}_2$ are updated using the rotation tensor $\underline{\underline{R}}$ of the polar decomposition applied to the initial vectors $\underline{e}_1^0$ and $\underline{e}_2^0$

$$\underline{e}_i = \frac{\underline{\underline{R}}.\underline{e}_i^0}{\left\|\underline{\underline{R}}.\underline{e}_i^0\right\|} \quad i = 1, 2 \tag{6}$$

Initially, the initial vectors of the two bases (Fiber and Green Naghdi) coincide and are orthogonal, but the fiber vectors do not remain so after deformation. Therefore, two orthogonal frames are defined, based on one of two fiber vectors. The first orthogonal frame is constructed from the first fiber vector $\underline{f}_1$ and the orthogonal unit vector $\underline{f}^2/\|\underline{f}^2\|$. The second orthogonal frame is based on the second fiber vector $\underline{f}_2$ and $\underline{f}^1/\|\underline{f}^1\|$. $B_{\underline{f}_1} = \left(\underline{f}_1; \underline{f}^2/\|\underline{f}^2\|\right)$ is the basis that refers to the first frame and $B_{\underline{f}_2} = \left(\underline{f}^1/\|\underline{f}^1\|; \underline{f}_2\right)$ is the basis that refers to the second one. $B_e = (\underline{e}_1; \underline{e}_2)$ refers the Green Naghdi basis.

Let θ_1 be the angle between the two current vectors $\underline{e}_1$ and $\underline{f}_1$ and θ_2 the angle between the vectors $\underline{e}_2$ and $\underline{f}_2$ (see Figure 2). The latter angles define the transformation matrices frome the Green Naghdi basis to the B_{f_i} basis.

$$[T]_i = \begin{bmatrix} \cos\theta_i & -\sin\theta_i \\ \sin\theta_i & \cos\theta_i \end{bmatrix} \quad i = 1, 2 \tag{7}$$

At each time step, the strain increment $[d\varepsilon]_e$ is determined by the explicit FE computation, expressed in the Green Naghdi frame. Then, the strain increment is converted to the two orthogonal fiber frames using the following expression:

$$[d\varepsilon]_{f_i} = [T]_i^T [d\varepsilon]_e [T]_i \quad i = 1, 2 \tag{8}$$

The direct strain increment $d\varepsilon_{11}^{f_1}$ in the direction of the fiber f_1 is calculated from the first component of $[d\varepsilon]_{f_1}$. In the second direction, the direct strain increment $d\varepsilon_{22}^{f_2}$ is equal to the second component of $[d\varepsilon]_{f_2}$, whereas the in-plane shear strain increment, defined as the angle between the warp and weft yarns, is calculated by the sum of the components of shear strain increments of $[d\varepsilon]_{f_1}$ and $[d\varepsilon]_{f_2}$.

$$\begin{cases} d\varepsilon_{11} = d\varepsilon_{11}^{f_1} \\ d\varepsilon_{22} = d\varepsilon_{22}^{f_2} \\ d\gamma = d\varepsilon_{12}^{f_1} + d\varepsilon_{12}^{f_2} \end{cases} \tag{9}$$

The constitutive equation is used to evaluate the stress increments in the two fiber frames:

$$[d\sigma]_{f_i} = [C_i]_{f_i} [d\varepsilon]_{f_i} \quad i = 1, 2 \tag{10}$$

In the orthogonal fiber frames, the elastic matrices are given by the tensile modulus in each of the fiber directions E_1, E_2 and the in-plane shear modulus G_{12}:

$$[C_1]_{f_1} = \begin{bmatrix} E_1 & 0 & 0 \\ 0 & 0 & 0 \\ 0 & 0 & G_{12} \end{bmatrix} \; ; \; [C_2]_{f_2} = \begin{bmatrix} 0 & 0 & 0 \\ 0 & E_2 & 0 \\ 0 & 0 & G_{12} \end{bmatrix} \tag{11}$$

Uniaxial and biaxial loadings on woven reinforcements lead to rigidity that increases gradually with tension due to the undulation of the fibers. This phenomenon has been studied for example in [59] and [60]. However, it has been shown that the modification of the deformed geometry due to this phenomenon is not very important in the case of classical reinforcements which are not much undulated. This was shown for example in [60]. In this study, Young's modulus was considered constant for reasons of simplicity and because

the undulations do not fundamentally change the phenomenon studied here, i.e. the consequences of whether or not the fibre directions are updated. The shear modulus G_{12} is non-linear, its expression is specified in section 5.2.

The stresses in the fiber frame are updated according to the work by Hughes and Winget [49] by the following expression:

$$\left[\underline{\underline{\sigma}}^{n+1}\right]_{f_i^{n+1}} = \left[\underline{\underline{\sigma}}^{n}\right]_{f_i^{n}} + \left[d\underline{\underline{\sigma}}\right]_{f_i^{n+1/2}} \quad i = 1, 2 \tag{12}$$

Finally, the stress expressed in the Green Naghdi frame is given as:

$$\left[\underline{\underline{\sigma}}^{n+1}\right]_{e^{n+1}} = [T]_1 \left[\underline{\underline{\sigma}}^{n+1}\right]_{f_1^{n+1}} [T]_1^T + [T]_2 \left[\underline{\underline{\sigma}}^{n+1}\right]_{f_2^{n+1}} [T]_2^T \tag{13}$$

3. Fiber orientation: Element values transfer

The forming simulation is performed within the FE code Abaqus using the hypoelastic law described in the section 2. It gives several output data such as the stress, the strain, the displacement and the shear angle. To extract all the necessary data (the deformed nodal coordinates, integration point coordinates, the local material directions) which will be used to develop the model of the final composite structure analysis, a python script has been developed. The code iteratively loops through every element in the deformed geometry, obtained from the forming simulation in order to create a local frame in each element. In the cured composite, the material behavior is given in an orthonormal frame. The warp and weft yarn directions coincide with the element side. It is assumed that the fiber elongations are small. Consequently, the frame based on the bisector of the warp and weft directions after deformation is orthogonal (Figure 3). In this orthonormal frame, the symmetries cause the mechanical behavior of the cured composite to be orthotropic.

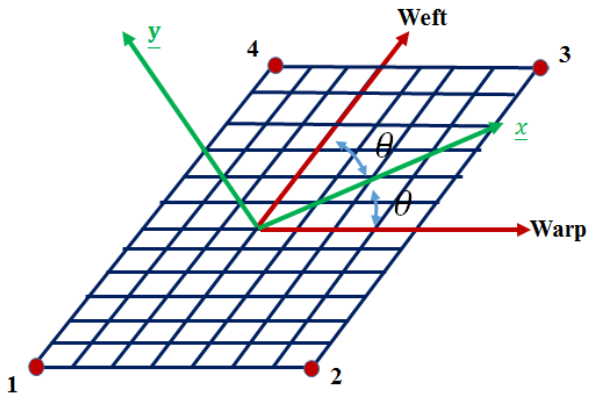

Figure 3: Local orthogonal frame in a sheared element

4. Structural analysis considering the fiber reorientations

Due to the in-plane shear strains during the forming of the prepreg composite, the yarns in the cured fabric are not perpendicular. Consequently, it is necessary to develop an elastic model that takes into account the reorientation of the fibers. To that end, some analytical formulation as the sub-plies model [61],the Ishakawa and Chou model [62] and the Naik model [63] can be used. These approaches were developed at the mesoscopic scale by using a REV of the woven composite and the stratify theory of UD composites.

In the present work, a simple elastic orthotropic model in the bissector frame was considered for the cured sheared woven composite. It was obtained as the superposition of tensile stiffness in the warp and weft directions and of an in plane-shear stiffness representing the matrix.

The warp and weft directions are placed at an angle θ (resp $-\theta$) of the x- axis coinciding with the bisector of the warp and weft directions in each element. There, $B_b = (\underline{x}, \underline{y})$ denotes the bisector basis (an orthogonal frame having the first vector as the bisector between the two fiber directions). $B_{f_1} = \left(\underline{f}_1, \underline{f}_1^{\perp}\right)$ is the first basis with the first vector in the warp direction. $B_{f_2} = \left(\underline{f}_2, \underline{f}_2^{\perp}\right)$ is the second basis that tracks the weft vectors (Figure 4). Note that the third vector is common for the three frames, and is perpendicular to the plane.

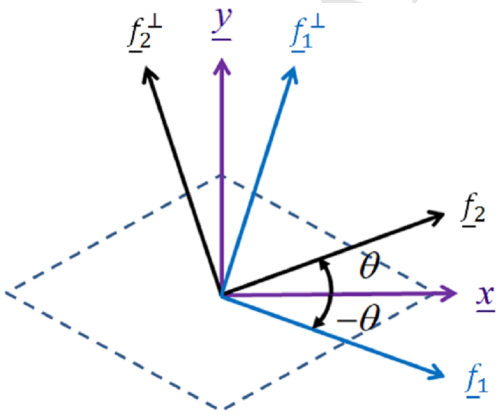

Figure 4: Orientation of the bisector and fiber axes

The relationship between the components of the stress in the bisector basis and the components of the stress written in the fiber basis obtained by a rotation about the third vector with an angle θ, can be given as follows:

$$\begin{bmatrix} \sigma_{11} \\ \sigma_{22} \\ \sigma_{12} \end{bmatrix}_{B_{f_1}} = [T(\theta)] \begin{bmatrix} \sigma_{11} \\ \sigma_{22} \\ \sigma_{12} \end{bmatrix}_{B_b} \tag{14}$$

and

$$[T(\theta)] = \begin{bmatrix} c^2 & s^2 & 2cs \\ s^2 & c^2 & -2cs \\ -cs & cs & c^2 - s^2 \end{bmatrix} \tag{15}$$

there, $c = cos(\theta)$ and $s = sin(\theta)$.

$T(\theta)$ presents the transformation matrix between B_b and B_{f_1}. The transformation matrix between B_b and B_{f_2} is obtained by changing θ to $-\theta$. Hence,

$$\begin{bmatrix} \sigma_{11} \\ \sigma_{22} \\ \sigma_{12} \end{bmatrix}_{B_{f_2}} = [T(-\theta)] \begin{bmatrix} \sigma_{11} \\ \sigma_{22} \\ \sigma_{12} \end{bmatrix}_{B_b} \tag{16}$$

The stiffness matrix due to the warp yarns in direction $\underline{f}_1$, expressed in the frame B_{f_1} is:

$$[C]_{B_{f_1}} = \begin{bmatrix} E_1 & 0 & 0 \\ 0 & 0 & 0 \\ 0 & 0 & 0 \end{bmatrix} \tag{17}$$

The stiffness matrix due to the warp yarns in direction $\underline{f}_2$, expressed in the frame B_{f_2} is:

$$[C]_{B_{f_2}} = \begin{bmatrix} E_2 & 0 & 0 \\ 0 & 0 & 0 \\ 0 & 0 & 0 \end{bmatrix} \tag{18}$$

The stiffness due to the resin is considered as isotropic.

$$[C]_m = \begin{bmatrix} \frac{E_m}{1-{\nu_m}^2} & \frac{\nu_m E_m}{1-{\nu_m}^2} & 0 \\ \frac{\nu_m E_m}{1-{\nu_m}^2} & \frac{E_m}{1-{\nu_m}^2} & 0 \\ 0 & 0 & \frac{E_m}{2(1+\nu_m)} \end{bmatrix} \tag{19}$$

E_m and ν_m are respectively the Young modulus and the Poisson ratio of the matrix. The cured composite is considered as an orthotropic elastic material in the bisector frame. The tensile stresses along both fiber directions are computed by using the constitutive matrices, given by Equation 17 and Equation 18:

$$[\sigma]_{f_\alpha} = [C]_{f_\alpha} [\varepsilon]_{f_\alpha} \tag{20}$$

These stresses are transferred to the bisector frames using Equation 14 and Equation 16. The state stress due to resin is calculated directly in the bisector frame. Finally, the composite stress state is obtained in the bisector basis by calculating the sum of the three stresses. In addition to the membrane behavior presented above, shell stiffness is added based on the standard membrane shell relation since the composite is hardened.

5. Composite structural simulations taking into account the forming process

5.1. Bias Extension Test

The bias extension test consists in streching a rectangular thermoplastic prepreg specimen with a length greater than twice the size of the width ($70 \times 210 mm^2$ in the present test). The two groups of yarns in this specimen are orientated $\pm 45°$ to the direction of the tensile force (Figure 5). The purpose of the test

is to obtain a pure shear state in the central zone by using a simple tension test. The bias extension test targets dry composite reinforcements (without resin) and prepregs when the matrix is melted. When the specimen is stretched from L to (L+d), the deformed specimen contains three different zones Z_A, Z_B and Z_C. The central zone Z_A is characterized by a pure shear deformation $\gamma = \pi - \alpha$. In the zone Z_C there is no deformation and the shear angle γ is zero. In zone Z_B the value of γ is half of that of zone Z_C. In the central zone Z_C, the shear angle can be expressed analytically as a function of the displacement of the tensile machine d and the length of the central zone D [64, 65]. The shear angle can be calculated as

$$\gamma = \frac{\pi}{2} - 2.a\cos\left(\frac{D+d}{\sqrt{2}D}\right) \tag{21}$$

where, D is the difference between the length and width of the test specimen in the undeformed state.

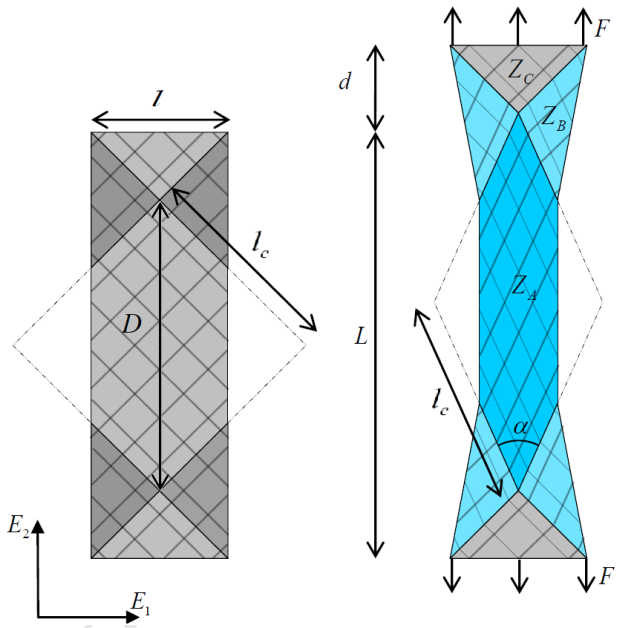

Figure 5: Illustration of the initial and deformed specimen under a bias-extension test

The material used in these experiments is a commercially available pre-consolidated plate provided by Solvay. The prepreg is made up of 8-Harness Satin glass/PA66 thermoplastic prepregs [11]. The specimen is placed in an universal tensile test machine within an isothermal oven (Figure 6.a) in order to reach the forming temperature. In the case of the PA66 matrix, the test temperature is 300^oC (slightly above the melting temperature). When the resin's temperature reaches the melting point, the sample's thickness decreases and the specimen can slide over the clamping system. For that, special jaws equipped with a spring system and a set of dog point screws were used [66].

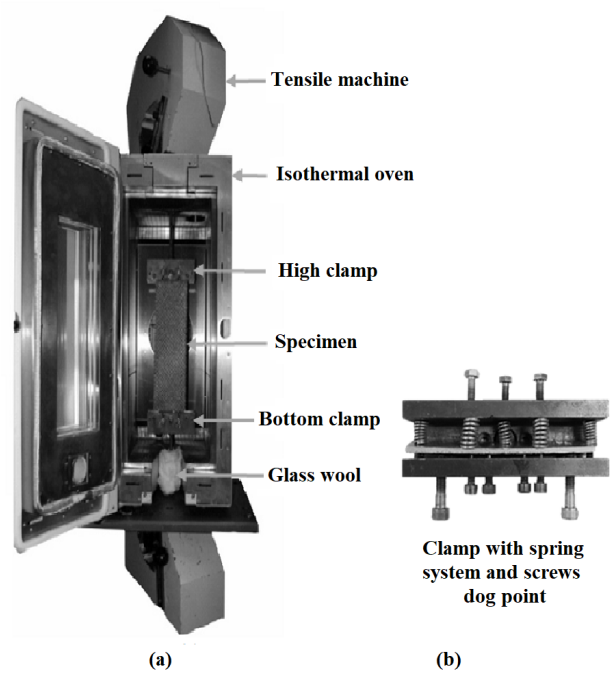

Figure 6: (a) Experimental setup and (b) clamp system

The total displacement was $d = 50mm$, and this displacement corresponds to a theoretical shear angle $\gamma = 57°$. Figure 7 shows the deformed specimen at the end of the bias extension test. In addition, the Figure 7 clearly portrays the three zones(Z_A, Z_B and Z_C), indicating that the prepreg specimens followed the bias extension test assumptions.

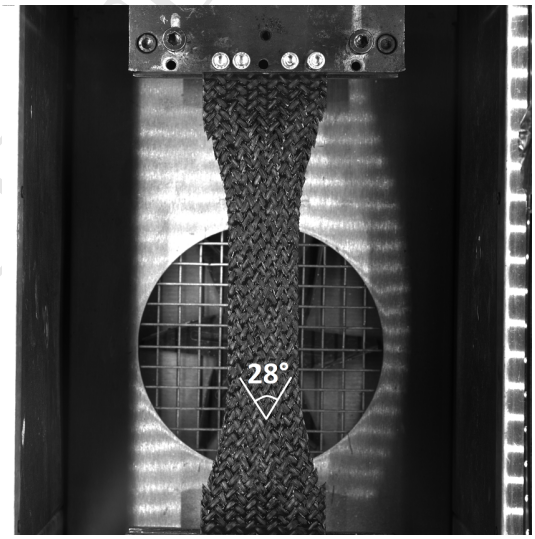

Figure 7: Deformed sample

After the process (here, the bias extension test) and a cooling phase to get the thermoplastic resin to a

solid state, a tensile test (longitudinal direction) was applied on the thermoformed hardened composite, in which the yarn directions had been modified by the thermoforming.

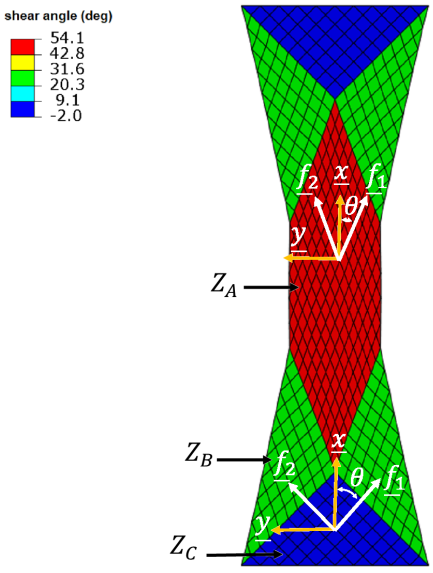

Figure 8: Simulation of the bias extension test- shear angle (degree)

The simulation of the bias test was performed by using the rate constitutive law developed in section 2. In the intial state, the elements and the yarns were oriented at 45^o relative to the load axis. The shear angle after deformation corresponded to Equation 21. Figure 8 shows the different zones and values of shear angle in the bias extension test simulation. In these three different zones, the plane shear is constant and there is no transition between the zones. Experimentally, there are transition areas. This lack of transition in the simulation result is related to the first gradient behaviour model that is used. To make these transition zones appear, second gradient models and discrete beam models have recently been developed [44]. These allow the stiffness of the fibres to be taken into account. Nevertheless, the angle values obtained by the simulation of the first gradient are in good agreement with the experiments in the central part of the specimen.

Figure 9 presents the evolution of the numerical and theoretical shear angle in the central zone, versus the displacement of the tensile machine during the bias extension test. The analytical and numerical results are in good agreement.

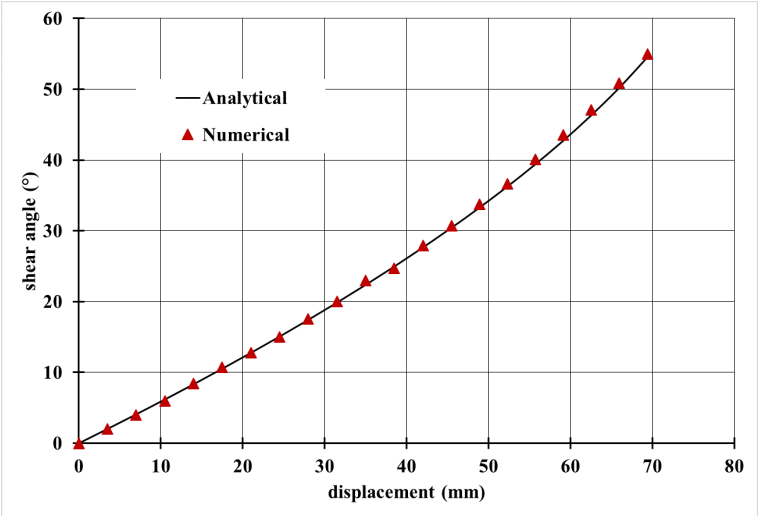

Figure 9: Comparison of the numerical and analytical results of the shear angle vs the displacement

To analyze the effect of the fiber reorientation, a comparison was carried out between the experiment and the simulation of a tensile test on a specimen after a bias extension test. In the simulation, the reorientation of the fiber was either taken into account or neglected. The fiber orientation in elements in the different zones can be seen in Figure 8.

Bias extension tests followed by a tensile test were performed for four cured specimens and Figure 10 shows the load versus displacement curves. The error bars are given in the Figure 10. F.E analyses were carried out either taking into account or neglecting the reorientation of the fibers. The simulation without considering the process effect (the fiber directions were assumed to be orthogonal) underestimated the stiffness of the specimen, whereas that taking into account the fiber reorientation showed a fairly good agreement with the experimental tests in the linear part.

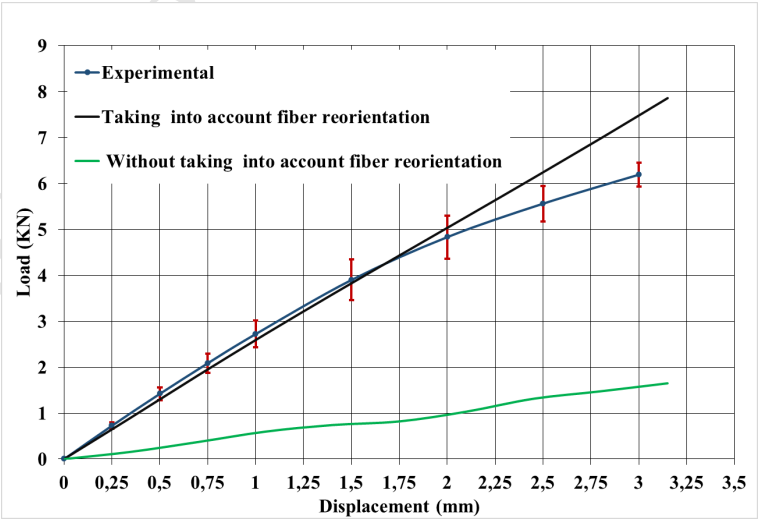

Figure 10: Force vs displacement for bias extension tests followed by a tensile test

5.2. Hemispheric forming followed by a loading on the cured composite part

Hemispherical stamping has often been used as a reference test for forming woven composites [17, 67–69]. The simulation of the hemispherical forming tests were carried out using the ABAQUS Explicit code and the rate constitutive law presented in section 2 for the composite reinforcement blank ($300X300mm^2$). The rate constitutive law was taken into account via a user subroutine (VUMAT).

The simulations presented in sections 5.2 (hemisphere) and 5.3 (double dome) concern a balanced commingled glass/polypropylene plain weave fabric produced by Vetrotex Saint-Gobain which was studied in the benchmark on composite reinforcement mechanical properties reported in [64]. The area density of the fabric is 743g/m2, the yarn linear density is 1870 tex and the thickness 1.2 mm (further information can be found in [64]).

The model has four parts (Figure 11). The punch is presented as a hemispherical tool with a radius of 78 mm. The die has a 80 mm radius. The third part is the blank holder presented as a flat disk. The holder is used to prevent the onset of wrinkles. The die, punch and holder are meshed by using 3-D triangular rigid elements (R3D3).

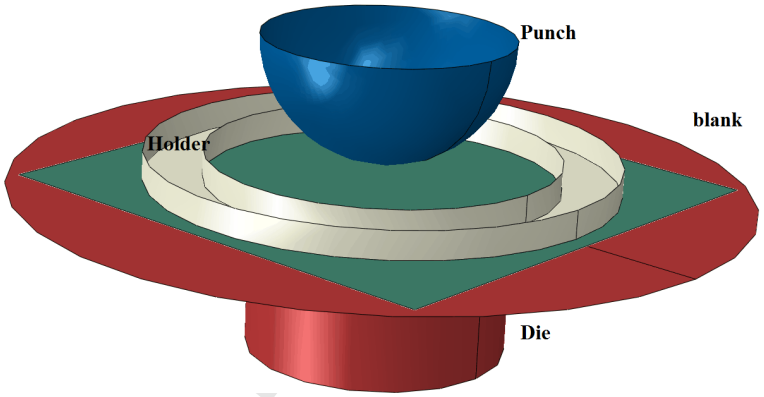

Figure 11: Hemispherical stamping: tool geometry

The material properties used in this simulation based on the approach described in section 2, are as follows:

- The tensile modulus in the warp and weft fiber directions $E_{11} = E_{22} = 35400MPa$
- The in-plan shear modulus is given by (MPa):

$$G_{12}(\gamma) = 8.48\gamma^4 - 12.0972\gamma^3 + 6.1275\gamma^2 - 0.83\gamma + 0.051 \quad (22)$$

The velocity of the punch was sufficiently low for the effort of inertia to be neglected. The interactions between the reinforcement and the tools were modeled by a Coulomb friction law. The coeffecient of friction was assumed to be constant and was set at 0.3. Figure 12 shows the shear angle distribution at the end of the forming simulation for two different loads on the blank holder (200N and 100N). The maximum value of

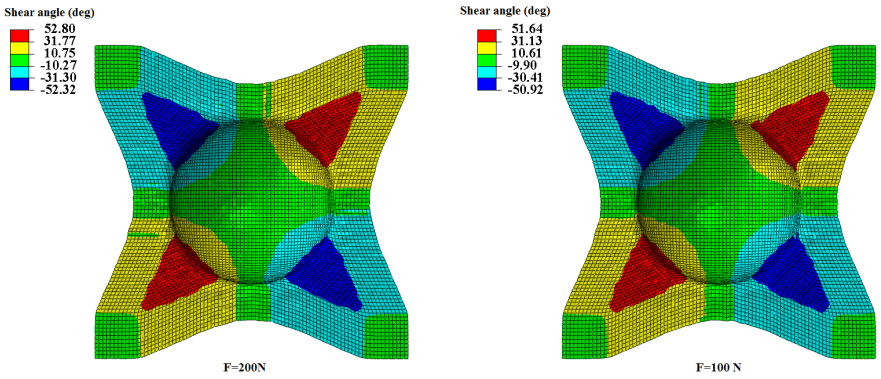

Figure 12: Shear angle after forming (deg)

the shear angle was about 50° in zone A. The magnitude of the binder force had little effect on the maximum shear angle. In order to highlight the effect of the binder force on the draped part, an asymmetric blank holder configuration was considered (Figure 13). The force is applied at the two diagonals of the blank.

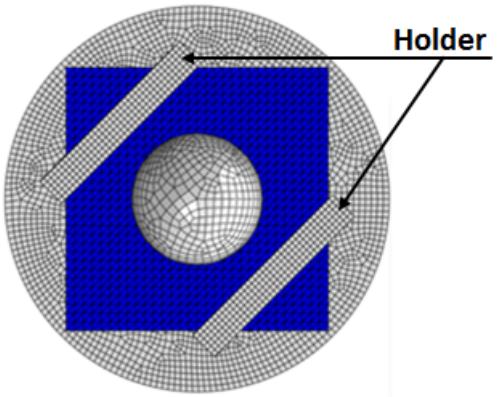

Figure 13: Non-axisymmetric blank holder

Figure 14 shows that asymmetric blank holder loads affected the result of the forming, in particular the shear-angle distribution. After this forming process, a structural analysis was performed on the deformed cured composite part taking into account the reorientation of the fibers. The FE structural analysis of the cured composite is a small deformation calculation that should be performed with a fine mesh size, particularly to obtain relevant stress fields in highly loaded areas. For purposes of simplicity, the same mesh was used in this work for the simulation of the forming and for the structural analysis of the hardened composite. This does not change the conclusions of this study.

The in-plane shear due to forming was large in some regions. Consequently, the stiffness of the cured composite was significantly changed. To show the effect of the fiber reorientation on the mechanical behavior of the part, a structural analysis was performed for the loading on the hardened composite part after forming (Figure 15). A displacement was applied to one side of the deformed hemisphere of the hardened composite,

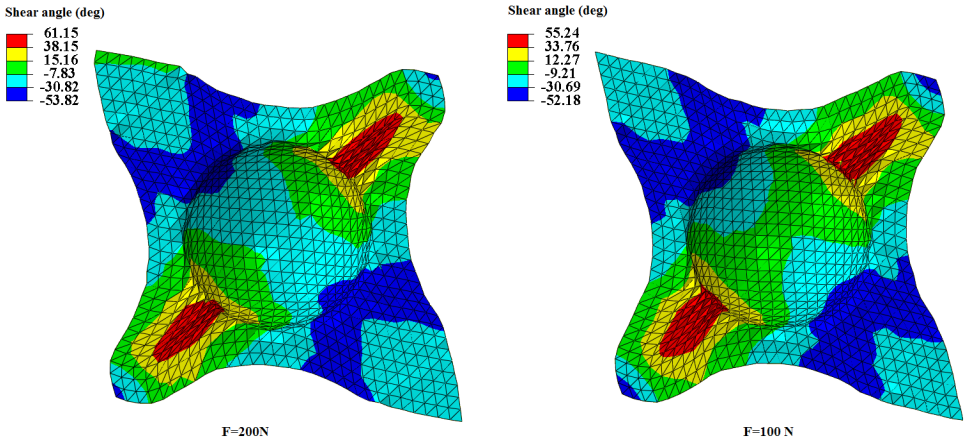

Figure 14: Shear angle after a forming with an asymmetric blank holder force

as shown in Figure 15. The Young's modulus of yarns was that given for the simulation of the forming process. The resin (polypropylene at room temperature) was assumed to be isotropic (Equation 19). The analysis was carried out by either taking into account or neglecting the reorientation of the fibers due to the shaping. When the analysis is carried out without taking into account fiber reorientation, the constitutive model is that of an orthotropic material whose orthotropic axes are those of the warp and weft yarns which here are assumed to be perpendicular and the shear modulus is that of the matrix. In this simulation, shell elements S3R were used.

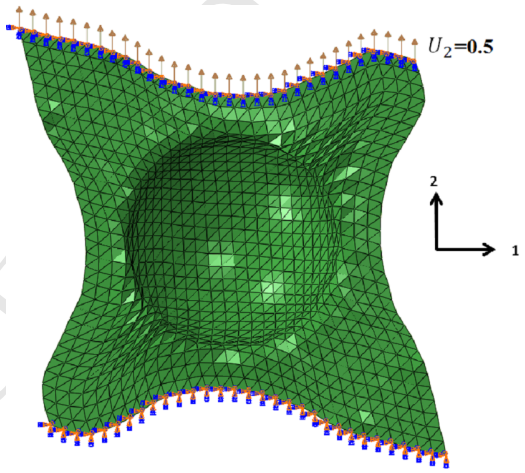

Figure 15: In plane loading of the hardened composite part

Figure 16 shows the stress state on the top layer of the composite shell when a 0.5 mm displacement was applied in direction 2 on the boundary according to Figure 15. The lower boundary was clamped.

The stress states that were achieved by taking into account or neglecting the reorientation of the fibers were found to differ. In particular, the direct stress in direction 2 is significantly larger when the fibers were assumed to be in directions 1 and 2 (without reorientation) than when the update of the fiber directions

was taken into account. This was confirmed by the calculation of the load on the edges in direction 2 in both cases (Figure 17). This global effort was much lower when an updated fiber orientation was taken into account.

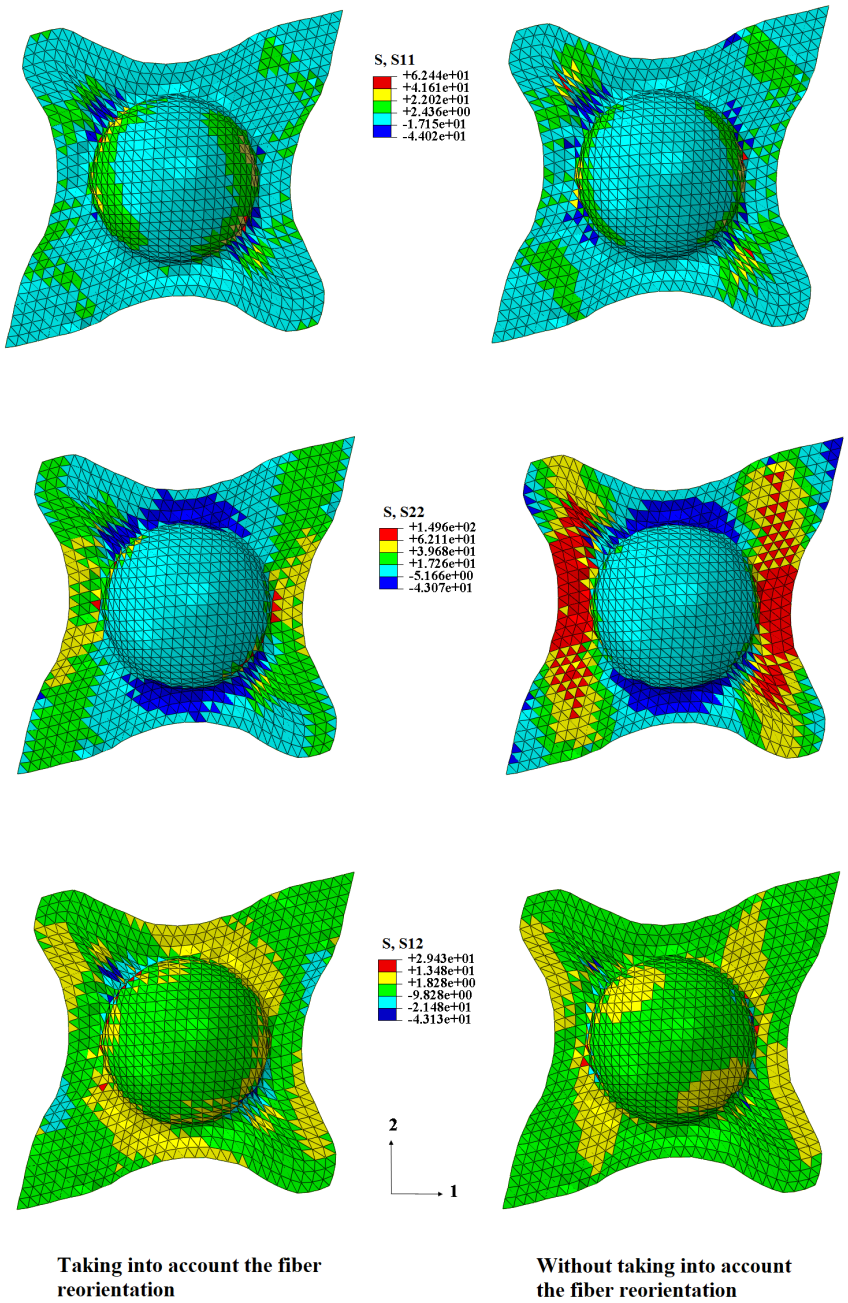

Figure 16: Stress distribution for the simulation taking into account or neglecting the fiber reorientation caused by forming (MPa)

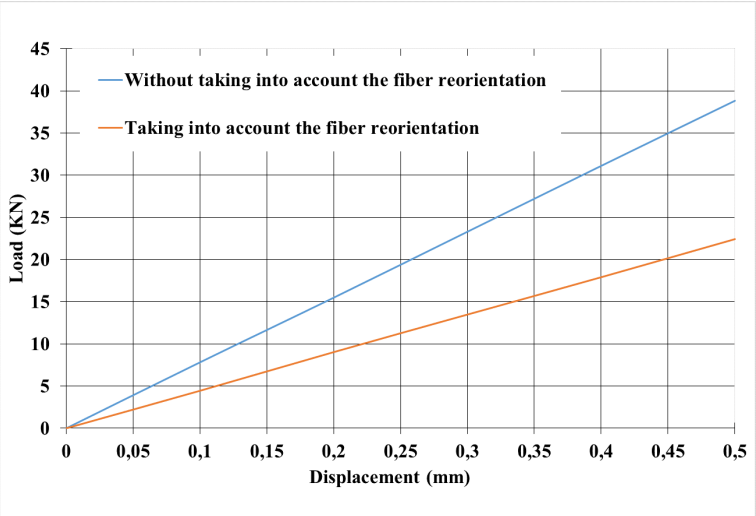

Figure 17: Force versus displacement U_2

5.3. Double dome forming followed by a loading on the cured composite part

The rate constitutive law presented in section 2 was applied for the simulation of a "double dome" forming benchmark [56, 70, 71]. Figure 18 shows the FE model of the double dome stamping process. The three tools used for the forming; i.e. blank holder, die and punch were assumed to be rigid bodies and they were meshed by using 3-D triangular rigid elements. The composite reinforcement blank was modeled in quarter symmetry. The intial dimensions of the fabric (quarter) was 235 mm x 135 mm. A constant 100N force was applied by the holder on the blank. The total punch stroke was equal to 60 mm. The interaction (tool/fabric) was modeled by using a 0.2 friction coefficient of the Coulomb law.

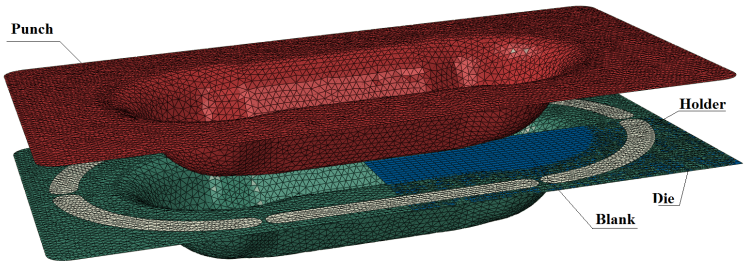

Figure 18: Double dome stamping simulation geometry

The forming simulations were carried out on 0°/90° fabric, and the simulation results for the shear angle distribution in 0°/90° fabric are presented in the Figure 19-a. For the 0°/90° fabric, the maximum shear angle value was approx 42.01° in the transition region between the double dome curve surface and the flat areas of the deformed woven fabric.

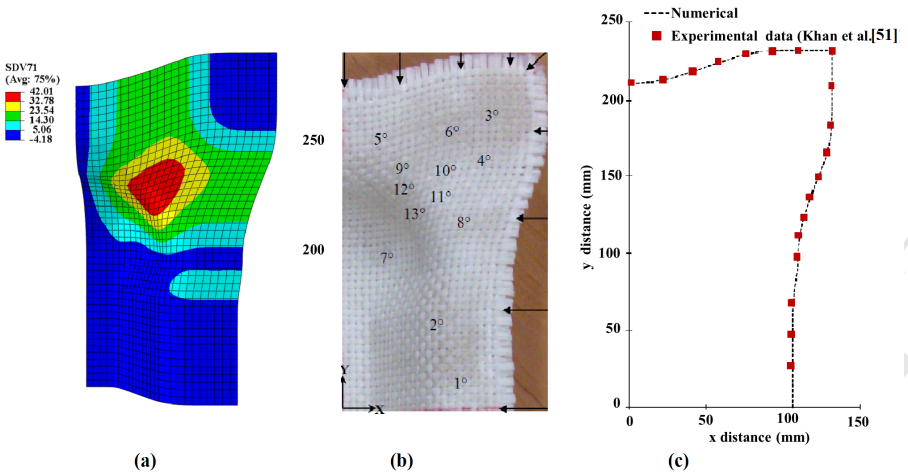

Figure 19: (a) Shear angle after double dome forming (b) Location of points for shear angle measurements for 0°/90° orientation (c) Deformed boundary profile comparison

Figure 19-c presents the numerical and experimental deformed boundary profiles after the forming. The experimental data were taken from the work of Khan et al [56]. As shown in the Figure 19-c, the deformed boundary profile was consistent between the simulation results and the experimental data.

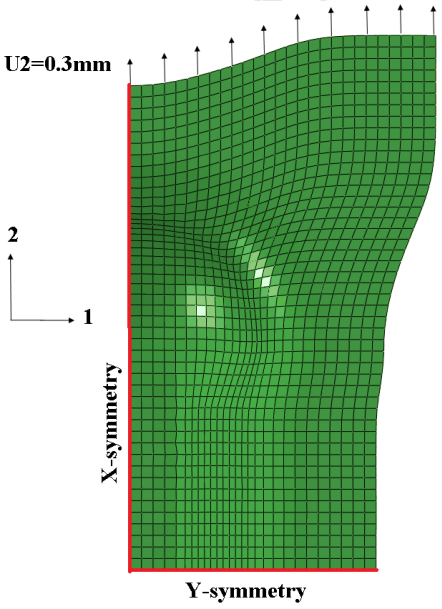

Figure 20: Loading of the hardened double dome

After the forming simulation, a structural analysis was performed on the hardened double dome composite. The final model of the draped double dome (in the case of a 0°/90° fabric) was exported and used in the structural analysis. Figure 20 shows the boundry conditions applied on the double dome. A 0.3mm displacement was applied on the top side of the hardened double dome composite. Symmetry boundry

conditions were employed on the quarter of the hardened double dome part. Two analyses were carried out: The first one took into account the fiber reorientation due to the forming process, whereas the second was performed without considering this fiber reorientation (i.e. orthogonal fabric).

Figure 21 shows the tensile load-displacement curves for the two simulations (taking into account or neglecting the change of the fiber orientation due to the forming). The difference between the two FE analyses shows the effect of considering the reorientation fiber caused by the forming on the global stiffness of the cured double dome composite. From Figure 21, it can be seen that not taking into account the fiber reorientation in the structural analysis clearly led to an overestimation of the global effort.

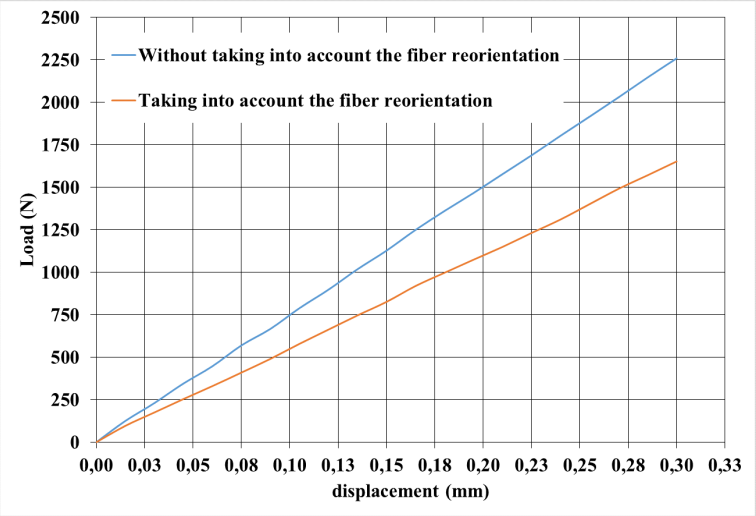

Figure 21: Load-displacement curve from the simulation results (taking into account or neglecting the fiber reorientation due to the forming)

Figure 22 shows the stress state on the top layer of the composite shell. Looking at the stress in this test, it confirmed that the reorientation fiber affectd the stress state obtained through the structural analysis. For example, in direction 2, the direct stress was more important in the case of the orthogonal fabric (without consideration of the fiber reorientation) because one of the yarn directions was in the direction of loading. In addition, in regions with very low shear angles ($\simeq 0$), the stresses were almost equal in the two simulations. The comparison between the simulations showed that the mechanical properties, such as stifness, were thus affected by the fiber reorientations.

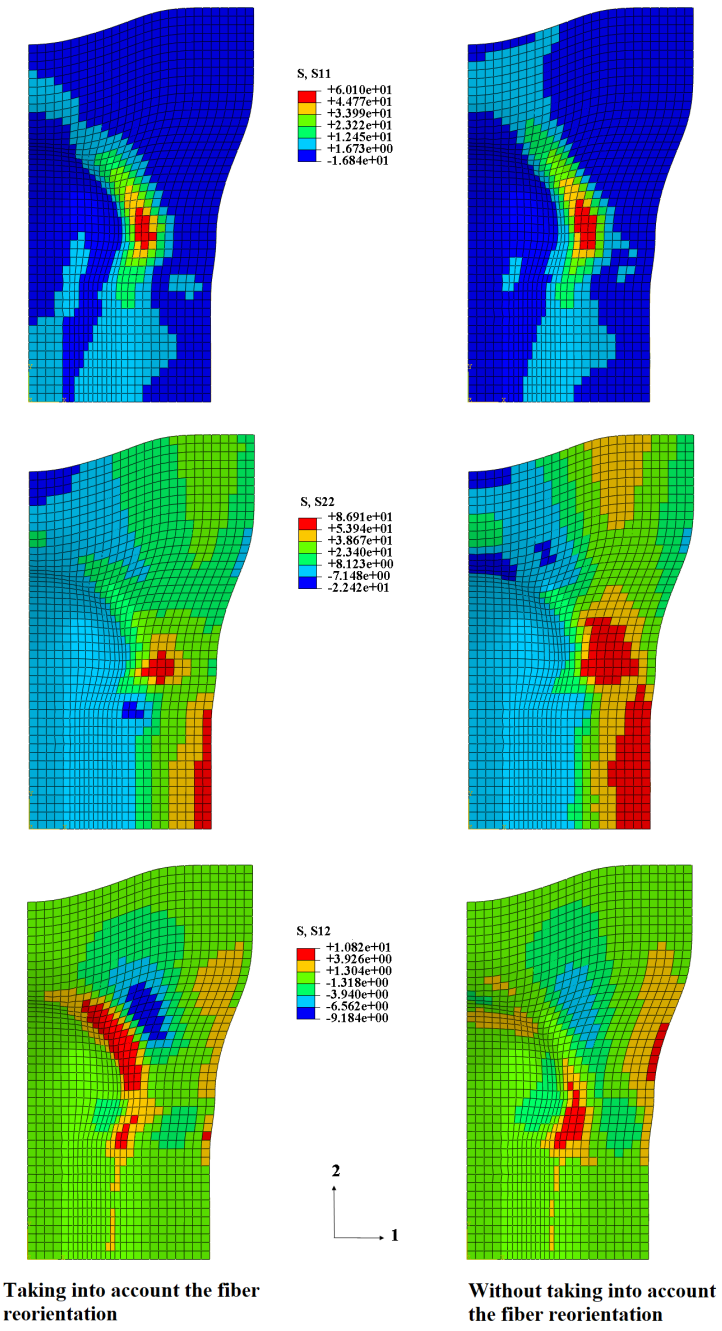

Figure 22: Stress distributions for the simulation of a hardened double-dome composite: (left) without taking into account the fiber reorientation (right), and taking into account the fiber reorientation (MPa)

Conclusion

During the preforming and the thermoforming processes, the woven composite fabrics were sheared to obtain the final geometry. The reorientation of the fiber yarns significantly affected the strength and the stiffness of the final composite. The major highlights of this contribution consisted in taking into consideration

the effect of the fiber reorientation of the composite during the forming process and its consequences on the structural reponse of the final composite. To figure out the inital shearing state, a hypoelastic model was used to simulate the forming process. The warp and weft fiber directions were determined by the forming simulation. A simple orthotropic model was developed in the bissector frame of the fiber directions after forming. This approach showed good agreement with experimental results in the case of the tension of sheared specimens by a bias extension test. In addition, the results of the tensile simulation on hemispherical and double dome geometries (taking into account the fiber reorientation) clearly pointed at the important effect of the shear angle on the stiffness of the composite part.

The fiber orientations affect other properties of the composite parts such as the thickness value and the fiber volume fraction. Moreover, other defects (such as wrinkles, porosity) could appear, during the manufacturing process, thereby affecting the performance of the final workpiece. In future work, it would be pertinent to feed the present model with other kinds of defects in order to refine the response prediction of the composite structural analysis.

Acknowledgements

The authors would like to express their gratitude to the company PSA for the financial support and for helpful discussions.

[1] E. R. Fuchs, F. R. Field, R. Roth, R. E. Kirchain, Strategic materials selection in the automobile body: Economic opportunities for polymer composite design, Composites science and technology 68 (9) (2008) 1989–2002.

[2] K. Friedrich, A. A. Almajid, Manufacturing aspects of advanced polymer composites for automotive applications, Applied Composite Materials 20 (2) (2013) 107–128.

[3] P. Mårtensson, D. Zenkert, M. Åkermo, Effects of manufacturing constraints on the cost and weight efficiency of integral and differential automotive composite structures, Composite structures 134 (2015) 572–578.

[4] G. Koronis, A. Silva, M. Fontul, Green composites: a review of adequate materials for automotive applications, Composites Part B: Engineering 44 (1) (2013) 120–127.

[5] V. S. Balakrishnan, H. Seidlitz, Potential repair techniques for automotive composites: A review, Composites Part B: Engineering 145 (2018) 28 – 38.

[6] B. Vieille, W. Albouy, L. Chevalier, L. Taleb, About the influence of stamping on thermoplastic-based composites for aeronautical applications, Composites Part B: Engineering 45 (1) (2013) 821–834.

[7] S. Haanappel, R. Ten Thije, U. Sachs, B. Rietman, R. Akkerman, Formability analyses of uni-directional and textile reinforced thermoplastics, Composites Part A: Applied science and manufacturing 56 (2014) 80–92.

[8] H. Lessard, G. Lebrun, A. Benkaddour, X.-T. Pham, Influence of process parameters on the thermostamping of a [0/90] 12 carbon/polyether ether ketone laminate, Composites Part A: Applied Science and Manufacturing 70 (2015) 59–68.

[9] R. Akkerman, S. Haanappel, Thermoplastic composites manufacturing by thermoforming, in: Advances in Composites Manufacturing and Process Design, Elsevier, 2015, pp. 111–129.

[10] A. Margossian, S. Bel, R. Hinterhoelzl, On the characterisation of transverse tensile properties of molten unidirectional thermoplastic composite tapes for thermoforming simulations, Composites Part A: Applied Science and Manufacturing 88 (2016) 48–58.

[11] E. Guzman-Maldonado, N. Hamila, N. Naouar, G. Moulin, P. Boisse, Simulation of thermoplastic prepreg thermoforming based on a visco-hyperelastic model and a thermal homogenization, Materials & Design 93 (2016) 431–442.

[12] N. A. Jayasree, A. Airale, A. Ferraris, A. Messana, L. Sisca, M. Carello, Process analysis for structural optimisation of thermoplastic composite component using the building block approach, Composites Part B: Engineering 126 (2017) 119–132.

[13] P. Hubert, A. Poursartip, Aspects of the compaction of composite angle laminates: an experimental investigation, Journal of Composite Materials 35 (1) (2001) 2–26.

[14] K. Potter, M. Campbell, C. Langer, M. Wisnom, The generation of geometrical deformations due to tool/part interaction in the manufacture of composite components, Composites part A: applied science and manufacturing 36 (2) (2005) 301–308.

[15] A. A. Skordos, C. M. Aceves, M. P. Sutcliffe, A simplified rate dependent model of forming and wrinkling of pre-impregnated woven composites, Composites Part A: Applied science and manufacturing 38 (5) (2007) 1318–1330.

[16] A. Rashidi, A. Milani, A multi-step biaxial bias extension test for wrinkling/de-wrinkling characterization of woven fabrics: Towards optimum forming design guidelines, Materials & Design 146 (2018) 273–285.

[17] P. Boisse, N. Hamila, E. Vidal-Sallé, F. Dumont, Simulation of wrinkling during textile composite reinforcement forming. influence of tensile, in-plane shear and bending stiffnesses, Composites Science and Technology 71 (5) (2011) 683–692.

[18] P. Ouagne, D. Soulat, J. Moothoo, E. Capelle, S. Gueret, Complex shape forming of a flax woven fabric; analysis of the tow buckling and misalignment defect, Composites Part A: Applied Science and Manufacturing 51 (2013) 1–10.

[19] P. Boisse, N. Hamila, A. Madeo, Modelling the development of defects during composite reinforcements and prepreg forming, Phil. Trans. R. Soc. A 374 (2071) (2016) 20150269.

[20] A. Long, C. Rudd, A simulation of reinforcement deformation during the production of preforms for liquid moulding processes, Proceedings of the Institution of Mechanical Engineers, Part B: Journal of Engineering Manufacture 208 (4) (1994) 269–278.

[21] F. Van Der Weeën, Algorithms for draping fabrics on doubly-curved surfaces, International journal for numerical methods in engineering 31 (7) (1991) 1415–1426.

[22] K. Potter, Beyond the pin-jointed net: maximising the deformability of aligned continuous fibre reinforcements, Composites Part A: Applied Science and Manufacturing 33 (5) (2002) 677–686.

[23] T. Gereke, O. Döbrich, M. Hübner, C. Cherif, Experimental and computational composite textile reinforcement forming: A review, Composites Part A: Applied Science and Manufacturing 46 (2013) 1–10.

[24] C. J. Mitchell, L. M. Dangora, J. A. Sherwood, Investigation into a robust finite element model for composite materials, Finite Elements in Analysis and Design 115 (2016) 1–8.

[25] P. Bussetta, N. Correia, Numerical forming of continuous fibre reinforced composite material: A review, Composites Part A: Applied Science and Manufacturing 113 (2018) 12–31.

[26] L. Kärger, S. Galkin, C. Zimmerling, D. Dörr, J. Linden, A. Oeckerath, K. Wolf, Forming optimisation embedded in a cae chain to assess and enhance the structural performance of composite components, Composite Structures 192 (2018) 143–152.

[27] Y. Miao, E. Zhou, Y. Wang, B. A. Cheeseman, Mechanics of textile composites: Micro-geometry, Composites Science and Technology 68 (7-8) (2008) 1671–1678.

[28] D. Durville, Simulation of the mechanical behaviour of woven fabrics at the scale of fibers, International journal of material forming 3 (2) (2010) 1241–1251.

[29] P. Latil, L. Orgéas, C. Geindreau, P. J. Dumont, S. R. Du Roscoat, Towards the 3d in situ characterisation of deformation micro-mechanisms within a compressed bundle of fibres, Composites Science and Technology 71 (4) (2011) 480–488.

[30] B. El Said, D. Ivanov, A. C. Long, S. R. Hallett, Multi-scale modelling of strongly heterogeneous 3d composite structures using spatial voronoi tessellation, Journal of the Mechanics and Physics of Solids 88 (2016) 50–71.

[31] L. Daelemans, J. Faes, S. Allaoui, G. Hivet, M. Dierick, L. Van Hoorebeke, W. Van Paepegem, Finite element simulation of the woven geometry and mechanical behaviour of a 3d woven dry fabric under tensile and shear loading using the digital element method, Composites Science and Technology 137 (2016) 177–187.

[32] S. V. Lomov, D. S. Ivanov, I. Verpoest, M. Zako, T. Kurashiki, H. Nakai, S. Hirosawa, Meso-fe modelling of textile composites: Road map, data flow and algorithms, Composites Science and Technology 67 (9) (2007) 1870–1891.

[33] P. Badel, E. Vidal-Sallé, E. Maire, P. Boisse, Simulation and tomography analysis of textile composite reinforcement deformation at the mesoscopic scale, Composites Science and Technology 68 (12) (2008) 2433–2440.

[34] H. Bayraktar, D. Ehrlich, G. Scarat, M. McClain, N. Timoshchuk, C. Redman, Forming and performance analysis of a 3d-woven composite curved beam using meso-scale fea, Sampe Journal 51 (3) (2015) 23.

[35] S. A. Tabatabaei, Y. Swolfs, H. Wu, S. V. Lomov, Full-field strain measurements and meso-fe modelling of hybrid carbon/self-reinforced polypropylene, Composite Structures 132 (2015) 864–873.

[36] Y. Rahali, M. Assidi, I. Goda, A. Zghal, J.-F. Ganghoffer, Computation of the effective mechanical properties including nonclassical moduli of 2.5 d and 3d interlocks by micromechanical approaches, Composites Part B: Engineering 98 (2016) 194–212.

[37] D. Wang, N. Naouar, E. Vidal-Salle, P. Boisse, Longitudinal compression and poisson ratio of fiber yarns in meso-scale finite element modeling of composite reinforcements, Composites Part B: Engineering 141 (2018) 9–19.

[38] A. Spencer, Theory of fabric-reinforced viscous fluids, Composites Part A: Applied Science and Manufacturing 31 (12) (2000) 1311–1321.

[39] P. Harrison, W.-R. Yu, A. C. Long, Rate dependent modelling of the forming behaviour of viscous textile composites, Composites Part A: Applied science and manufacturing 42 (11) (2011) 1719–1726.

[40] E. Syerko, S. Comas-Cardona, C. Binetruy, Models for shear properties/behavior of dry fibrous materials at various scales: a review, International Journal of Material Forming 8 (1) (2015) 1–23.

[41] A. C. Long, Composites forming technologies, Elsevier, 2014.

[42] P. Boisse, Composite reinforcements for optimum performance, Elsevier, 2011.

[43] N. Hamila, P. Boisse, A meso–macro three node finite element for draping of textile composite preforms, Applied Composite Materials 14 (4) (2007) 235–250.

[44] M. dAgostino, I. Giorgio, L. Greco, A. Madeo, P. Boisse, Continuum and discrete models for structures including (quasi-) inextensible elasticae with a view to the design and modeling of composite reinforcements, International Journal of Solids and Structures 59 (2015) 1–17.

[45] G. Bardl, A. Nocke, M. Hübner, T. Gereke, M. Pooch, M. Schulze, H. Heuer, M. Schiller, R. Kupke, M. Klein, et al., Analysis of the 3d draping behavior of carbon fiber non-crimp fabrics with eddy current technique, Composites Part B: Engineering 132 (2018) 49–60.

[46] Y. Aimène, E. Vidal-Sallé, B. Hagège, F. Sidoroff, P. Boisse, A hyperelastic approach for composite reinforcement large deformation analysis, Journal of Composite materials 44 (1) (2010) 5–26.

[47] Y. Gong, X. Peng, Y. Yao, Z. Guo, An anisotropic hyperelastic constitutive model for thermoplastic woven composite prepregs, Composites Science and Technology 128 (2016) 17–24.

[48] A. Charmetant, E. Vidal-Sallé, P. Boisse, Hyperelastic modelling for mesoscopic analyses of composite reinforcements, Composites Science and Technology 71 (14) (2011) 1623–1631.

[49] T. J. Hughes, J. Winget, Finite rotation effects in numerical integration of rate constitutive equations arising in large-deformation analysis, International journal for numerical methods in engineering 15 (12) (1980) 1862–1867.

[50] T. Belytschko, W. K. Liu, B. Moran, K. Elkhodary, Nonlinear finite elements for continua and structures, John wiley & sons, 2013.

[51] X. Peng, J. Cao, A continuum mechanics-based non-orthogonal constitutive model for woven composite fabrics, Composites Part A: Applied Science and Manufacturing 36 (6) (2005) 859–874.

[52] W.-R. Yu, P. Harrison, A. Long, Finite element forming simulation for non-crimp fabrics using a non-orthogonal constitutive equation, Composites Part A: Applied Science and Manufacturing 36 (8) (2005) 1079–1093.

[53] P. Boisse, A. Gasser, B. Hagege, J.-L. Billoet, Analysis of the mechanical behavior of woven fibrous material using virtual tests at the unit cell level, Journal of materials science 40 (22) (2005) 5955–5962.

[54] P. Badel, E. Vidal-Sallé, P. Boisse, Large deformation analysis of fibrous materials using rate constitutive equations, Computers & Structures 86 (11) (2008) 1164–1175.

[55] P. Boisse, N. Hamila, F. Helenon, B. Hagège, J. Cao, Different approaches for woven composite reinforcement forming simulation, International Journal of Material Forming 1 (1) (2008) 21–29.

[56] M. Khan, T. Mabrouki, E. Vidal-Sallé, P. Boisse, Numerical and experimental analyses of woven composite reinforcement forming using a hypoelastic behaviour. application to the double dome benchmark, Journal of materials processing technology 210 (2) (2010) 378–388.

[57] Y. Dafalias, Corotational rates for kinematic hardening at large plastic deformations, Journal of Applied Mechanics 50 (3) (1983) 561–565.

[58] J. K. Dienes, On the analysis of rotation and stress rate in deforming bodieszur untersuchung der rotations-und spannungsgeschwindigkeit in sich deformierenden körpern, Acta mechanica 32 (4) (1979) 217–232.

[59] S. Kawabata, M. Niwa, H. Kawai, 3the finite-deformation theory of plain-weave fabrics part i: the biaxial-deformation theory, Journal of the textile institute 64 (1) (1973) 21–46.

[60] P. Boisse, M. Borr, K. Buet, A. Cherouat, Finite element simulations of textile composite forming including the biaxial fabric behaviour, Composites Part B: Engineering 28 (4) (1997) 453–464.

[61] T. Vu-Khanh, B. Liu, Prediction of fibre rearrangement and thermal expansion behaviour of deformed woven-fabric laminates, Composites Science and Technology 53 (2) (1995) 183–191.

[62] T. Ishikawa, T.-W. Chou, One-dimensional micromechanical analysis of woven fabric composites, AIAA J 21 (12) (1983) 1714–1721.

[63] N. Naik, P. Shembekar, Elastic behavior of woven fabric composites: Ilamina analysis, Journal of composite materials 26 (15) (1992) 2196–2225.

[64] J. Cao, R. Akkerman, P. Boisse, J. Chen, H. Cheng, E. De Graaf, J. Gorczyca, P. Harrison, G. Hivet, J. Launay, et al., Characterization of mechanical behavior of woven fabrics: experimental methods and benchmark results, Composites Part A: Applied Science and Manufacturing 39 (6) (2008) 1037–1053.

[65] P. Boisse, N. Hamila, E. Guzman-Maldonado, A. Madeo, G. Hivet, F. DellIsola, The bias-extension test for the analysis of in-plane shear properties of textile composite reinforcements and prepregs: a review, International Journal of Material Forming 10 (4) (2017) 473–492.

[66] E. Guzman-Maldonado, N. Hamila, P. Boisse, J. Bikard, Thermomechanical analysis, modelling and simulation of the forming of pre-impregnated thermoplastics composites, Composites Part A: Applied Science and Manufacturing 78 (2015) 211–222.

[67] L. Dong, C. Lekakou, M. Bader, Processing of composites: simulations of the draping of fabrics with updated material behaviour law, Journal of composite materials 35 (2) (2001) 138–163.

[68] L. Dong, C. Lekakou, M. Bader, Solid-mechanics finite element simulations of the draping of fabrics: a sensitivity analysis, Composites Part A: applied science and manufacturing 31 (7) (2000) 639–652.

[69] H. Lin, J. Wang, A. Long, M. Clifford, P. Harrison, Predictive modelling for optimization of textile composite forming, Composites Science and Technology 67 (15) (2007) 3242–3252.

[70] P. Harrison, R. Gomes, N. Curado-Correia, Press forming a 0/90 cross-ply advanced thermoplastic composite using the double-dome benchmark geometry, Composites Part A: Applied Science and Manufacturing 54 (2013) 56–69.

[71] W. Lee, J. Cao, Numerical simulations on double-dome forming of woven composites using the coupled non-orthogonal constitutive model, International Journal of Material Forming 2 (1) (2009) 145.